Check for updates

Nanoscale

Accepted Manuscript

This article can be cited before page numbers have been issued, to do this please use: J. Li, R. Pan, Y. Yang, Y. Wang, S. Li, Z. liu, Y. Su, B. Quan, Y. Li and C. Gu, *Nanoscale*, 2018, DOI: 10.1039/C7NR08646F.

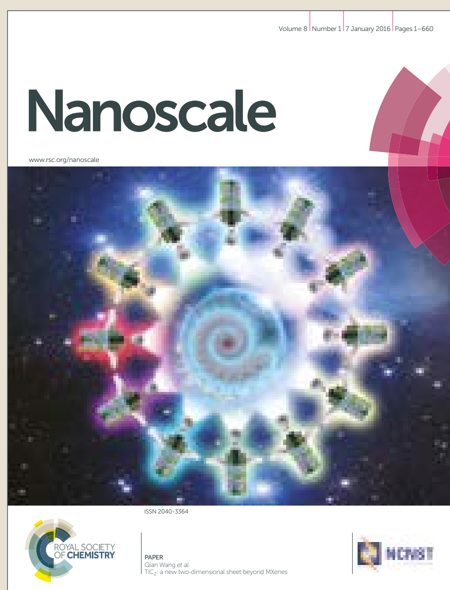

This is an Accepted Manuscript, which has been through the Royal Society of Chemistry peer review process and has been accepted for publication.

Accepted Manuscripts are published online shortly after acceptance, before technical editing, formatting and proof reading. Using this free service, authors can make their results available to the community, in citable form, before we publish the edited article. We will replace this Accepted Manuscript with the edited and formatted Advance Article as soon as it is available.

You can find more information about Accepted Manuscripts in the author guidelines.

Please note that technical editing may introduce minor changes to the text and/or graphics, which may alter content. The journal's standard Terms & Conditions and the ethical guidelines, outlined in our author and reviewer resource centre, still apply. In no event shall the Royal Society of Chemistry be held responsible for any errors or omissions in this Accepted Manuscript or any consequences arising from the use of any information it contains.

ROYAL SOCIETY OF CHEMISTRY

rsc.li/nanoscale

View Article Online
DOI: 10.1039/C7NR08646F

Nanocracking and Metallization Doubly-defined Large-scale 3D Plasmonic Sub-10nm-gap Arrays as Extremely Sensitive SERS Substrate

Ruhao Pan,[a,b] Yang Yang, [a] Yujin Wang, [a] Shuang Li, [b, c] Zhe Liu, [a] Yewang Su,[c] Baogang Quan, [a] Yunlong Li,[a] Changzhi Gu,[*,a,b,d] and Junjie Li[*,a,b]

[a] *Beijing National Laboratory for Condensed Matter Physics, Institute of Physics, Chinese Academy of Sciences, Beijing 100190, China. E-mail: jjli@iphy.ac.cn, czgu@iphy.ac.cn ; Tel: +86-10-82649097*

[b] *School of Physical Sciences, CAS Key Laboratory of Vacuum Physics, University of Chinese Academy of Sciences, Beijing 100049, China*

[c] *State Key Laboratory of Nonlinear Mechanics, Institute of Mechanics, Chinese Academy of Sciences, Beijing 100190, China*

[d] *Collaborative Innovation Center of Quantum Matter, Beijing, China*

Abstract

Faced with the technological difficulties in existing approaches to form nanoscale gaps, a convenient method to fabricate three-dimensional (3D) sub-10 nm Ag/SiN_x gap arrays was demonstrated, controlled by a combination of stress-induced nanocracking of SiN_x nanobridge and Ag nanofilm deposition. This scalable 3D plasmonic nanogap is specially suspended above a substrate, having tunable nanogap width and large height-to-width ratio to form a nanocavity underneath. As a surface-enhanced Raman scattering (SERS) substrate, such a 3D Ag/SiN_x nanogap shows a large Raman enhancement factor of $\sim 10^8$ and extremely high sensitivity for

Published on 02 January 2018. Downloaded by University of Reading on 07/01/2018 10:39:22.

Nanoscale Accepted Manuscript

View Article Online
DOI: 10.1039/C7NR08646F
Published on 02 January 2018. Downloaded by University of Reading on 07/01/2018 10:39:22.
Nanoscale Accepted Manuscript

detecting Rhodamine 6G (R6G) molecules even down to 10^{-16} M, indicating an extraordinary capability for single-molecule detection. Further, we verify that Fabry-Perot resonance occurs in the deep SiN_x nanocavity under the Ag nanogap, contributing prominently to a tremendous enhancement of local field at the Ag-nanogap zone and hence ultrasensitive SERS detection. This method circumvents the technological limitations to fabricate sub-10 nm metal nanogap with unique features for a wide application in important scientific and technological areas.

Keywords

Stress-induced cracking, suspended sub-10 nm nanogap, field enhancement, Surface enhanced Raman scattering, single molecular detection

Introduction

Metallic nanogaps have attracted considerable attention in recent years owing to their applicability in physics, chemistry, life sciences and environmental engineering.[1-5] They are widely used as the fundamental building blocks of microelectronic components such as ultrafast vacuum transistors, ultralow-power nanoelectromechanical switches,[6] and metallic-nanogap-electrode-based flexible electronics.[7] In addition, metallic nanogaps are promising for super-resolution imaging,[8] molecular electronic,[5, 9, 10] and sensor[11-13] applications. Among the diverse applications of metallic nanogaps, surface enhanced Raman spectroscopy (SERS) is one of the most important. SERS is a powerful analysis technique for ultra-sensitive detection.[14-22] SERS performance is governed by strong localized surface plasmon resonance (LSPR) on the noble metal nanoparticles or nanopatterns.[12, 23-25] Normally, the SERS enhancement factor (EF) of nanopatterns prepared by regular nanofabrication methods is just in the range of 10^5-10^6,[26, 27] which is not sufficient for single molecule detection (~10^7).[28] It has been shown that a metallic

View Article Online
DOI: 10.1039/C7NR08646F

Published on 02 January 2018. Downloaded by University of Reading on 07/01/2018 10:39:22.

nanogap can be capable of single-molecule detection.[17-19, 29] A sub-10 nm nanogap – wherein the electromagnetic field is strongly coupled in the narrow space, giving rise to much intense LSPR – is especially suited to such detection. Dimers and even multimeric structures with sub-10 nm nanogap have been realized by self-assembly of nanoparticles.[30] Recently, a sub-10 nm Au Bowie nanoantenna [18] and split-wedge antenna 3D nanostructure [31] were fabricated and reported, achieving an SERS EF on the order of 10^7, which was shown to be capable of single molecule detection. However, the detection limit for molecule concentration in these reports was normally around 10^{-10} M. Therefore, it is desirable to develop a SERS surface with an even lower detection limit, for high sensitivity and fast analysis at ultralow concentration, i.e. to design and fabricate a batter plasmonic nanogap.

Despite plasmonic nanogaps' advantages and wide applicability today, a remaining challenge is to fabricate scalable, reliable, and reproducible sub-10 nm metallic nanogaps. Traditional planar fabrication processes, such as ultraviolet lithography (UVL) and electron beam lithography (EBL), have sub-micron and 10 nm limitations, respectively.[12] Various methods have been developed to realize nanogaps in sub-10 nm scale. One effective method uses metallic particles or two dimensional (2D) thin films to build nanogaps.[32, 33] That is, the formation of sub-10 nm gaps should be enabled by graphene,[34] metal particles,[15, 35] or self-assemble.[36] However, these methods lack controllability, flexibility and stability; moreover they yield chemical pollution. To overcome these drawbacks in nanogaps based on nanoparticles, we had fabricated a metal-insulator-metal (MIM) structure via atomic layer deposition (ALD), controlling gap width by tuning the thickness of insulating inter-layer. The aim was to use this device for SERS measurement.[31] However, this type of filled nanogap does not function well as an electrode, limiting the utilization of nanogap that serves as a nanodevices combining multiple

Nanoscale Accepted Manuscript

View Article Online
DOI: 10.1039/C7NR08646F
Published on 02 January 2018. Downloaded by University of Reading on 07/01/2018 10:39:22.
Nanoscale Accepted Manuscript

functionalities,[37] such as molecule trapping and detection by tunneling current and high-sensitivity molecule identification by SERS. Recently, a new form of sub-10 nm gaps has appeared, namely, crack- or break-induced nanogaps. A number of methods have been put forward based on cracking or breaking procedures, including the mechanical break-junction method,[38] swelling-defined nanogaps,[7] and optical breakdown.[39] Scalable nanogap electrodes were fabricated on flexible substrates by swelling-induced cracks.[7] Note that the gap width in this case was over 50 nm, which is already beyond the scope of plasmon coupling. An approach called the crack-junctions (CJs) method was introduced to achieve nanogap arrays over a large area.[40] However, in addition to the inability to control the morphology of tips, the materials used for fabrication must be brittle, limiting the application of the resulting nanogaps. Although many creative methods have been proposed to fabricate nanogaps that offer good performance in either field enhancement or electron transport, parallel fabrication of stable and scalable sub-10 nm nanogap with control of the shape and width remains a challenge.

Here, we introduce a convenient stress-induced cracking method to fabricate a suspended 3D sub-10 nm Ag/SiN_x gap, consisting of an opposed pair of uniform tips, with good homogeneity over a large area. Each of the Ag/SiN_x nanogaps was fabricated based on stress-induced cracking of a SiN_x nanobridge, combined with a metallization process that includes EBL, and physical and chemical etching techniques, followed by depositing an Ag nanolayer that can easily tune the location and width of nanogap. This method circumvents the technological difficulties of the existing ways to fabricate nanoscale gaps. The suspended 3D Ag/SiN_x nanogaps exhibit some unique features such as highly controllable gap width within a range from sub-10nm to tens of nanometers, high ratio of gap-depth to gap-width， good array scalability, and wafer-scale fabrication. Moreover, we demonstrated an ultra-high SERS sensitivity of such suspended 3D

View Article Online
DOI: 10.1039/C7NR08646F

Published on 02 January 2018. Downloaded by University of Reading on 07/01/2018 10:39:22.

Nanoscale Accepted Manuscript

metallic sub-10nm nanogap, and the detection limit of Rhodamine 6G (R6G) molecules was found to be as low as 10^{-16} M and exceeding ~10^{8} in SERS enhancement factor (EF), sufficient for single molecule detection. Finite-difference time-domain (FDTD) simulation elucidated that Ag-nanogap, being sub-10 nm, contributes greatly to a tremendous local field enhancement for SERS. Further, as-obtained outstanding SERS EF is closely associated with Fabry-Perot resonances occurred in the deep SiN_x nanocavity under Ag-naogap. Thus we propose a feasible route to fabricate a large-area uniform 3D sub-10 nm nanogap array with a high SERS enhancement factor for promising applications in ultra-high sensitivity molecule sensing and hence its more unique features can be extended to many scientific and technological fields.

Experimental

Fabrication process

The 220 nm thick SiN_x was deposited on clean Si substrate by low pressure chemical vapor deposition (LPCVD) with a gas flow of NH_3: 30 sccm and SH_2Cl_2: 120 sccm, under 900 ℃. Then 200 nm thick PMMA was spin-coated on the SiN_x, and EBL (Ratih 150) was introduced to expose the nanobridge pattern. After that, RIE (NGP80, Oxford) was used to etch the PMMA pattern into the SiN_x layer, in which the gas flow was CHF_3: 50 sccm and O_2: 5 sccm, and pressure was maintained at 35 mTorr. The SiN_x was etched under 200 W power at 10 ℃ for 4 minutes. Then the sample was dipped into buffered oxide etching liquid (BOE) for 20 s to remove the oxide layer on the sample, and then the sample was cleaned by deionized water. The TMAH (25% w/w, Alfa Aesar) was heated to 95 ℃ in an oil bath and kept 1 hour for temperature to stabilize. Then the sample was etched by TMAH for 2 min, finally obtaining the suspended sub-10 nm nanogaps. The widths of the nanogaps were measured using SEM (Helios

View Article Online
DOI: 10.1039/C7NR08646F

600i, FEI). Silver film was deposited onto the SiN_x nanogap by magnetron sputtering system with ultra-high background vacuum (~10^{-10} Torr) to fabricate a metallic nanogap.

Simulation methods

The simulation of nanobridge breaking was based on the finite elements method (FEM). The nanobridge chosen for simulation has a width of 20 nm, but a length is set to zero to facilitate the simulation. By using FEM together with maximum normal stress strength theory, the maximum principle stress distribution was given, and the displacement distribution after stress release was calculated. Besides, the Finite-different time-domain **(**FDTD) method was employed to simulate the electric field distribution of the nanogaps. The Ag layer is 25 nm thick, while the SiN_x layers ranged from 50nm to 500 nm thick. The wavelength of the incidence light was set at 532 nm and propagated along the z-axis with the electric field polarized along the x-axis. Three monitors are placed perpendicular to X, Y, and Z axes respectively, to capture the field distribution fully. All the simulated boundaries were perfectly matched layers (PML) to avoid reflections. Taking advantage of the model mentioned before, the field distribution of the Ag nanogap and the Ag/SiN_x gap on Si substrate was calculated.

SERS measurements

R6G powders were dissolved in deionized water to prepare solutions of R6G. The samples were functionalized with molecules by immersion in the solutions for a certain time. The samples were taken out and washed by ethyl and DI water to remove the unbound molecules, and then dried with a flow of nitrogen. The SERS measurements were carried out on a micro-Raman spectrometer (Horiba/Jobin Yvon HR 800) equipped with a 532 nm laser as the excitation source. The laser was focused on the sample surface using a 100× lens (N A=0.9) with a 2μm in size. To protect the molecules from laser heating, the laser power was kept at 1 mW on the sample

Published on 02 January 2018. Downloaded by University of Reading on 07/01/2018 10:39:22.
Nanoscale Accepted Manuscript

View Article Online
DOI: 10.1039/C7NR08646F

surface, and the exposure time was 1 second. Each Raman spectrum was collected on a single gap, and repeatability was verified by collecting spectra on 5 randomly chosen gaps in different arrays.

Results and Discussion

Doubly controlled fabrication of Ag/SiN_x nanogap arrays

Our fabrication process employing stress-induced cracking starts with amorphous SiN_x film on a Si substrate. A schematic of the process, from nanobridge to nanogap, is shown in Figure 1a. First, a 220 nm amorphous SiN_x layer was specifically selected and deposited on a Si substrate because such a thick layer will not bend much during the subsequent technical processing of the metal/SiN_x film. The nanobridge pattern was fabricated by EBL process, and then the pattern was transferred onto the SiN_x film to serve as a mask during reactive ion etching (RIE). After that, tetramethylammonium hydroxide (TMAH) was used to etch the Si substrate alongside and underneath SiN_x nanobridge to form a suspended 3D nanobridge. As a result of the concentrated stress-release-induced cracking, a 3D suspended nanogap appeared in the middle of SiN_x nanobridge, having a width range from sub-10 nm to tens of nanometers. Finally, metallization accomplished by magnetron sputtering disposition to functionalize the nanogap. During the disposition, the nanogap can be narrowed to sub-10nm from tens of nanometers. This approach to fabricating nanogaps has better control of the nanogap width and is compatible with typical micro/nanofabrication processes for Si wafers. So it is well suited for preparation of large-area and customized nanogap arrays, making nanogap-based devices interesting for a wide range of possible application. Figure 1b presents an SEM image of typical as-fabricated metallic nanogap arrays, with two inset SEM images of a single SiN_x nanogap before and after metallization, in which the morphology and width of each metallic nanogap are nearly the same, demonstrating

Published on 02 January 2018. Downloaded by University of Reading on 07/01/2018 10:39:22.

Nanoscale Accepted Manuscript

View Article Online
DOI: 10.1039/C7NR08646F

Published on 02 January 2018. Downloaded by University of Reading on 07/01/2018 10:39:22.

good scalability and uniformity of the fabrication process employed in this work. Another important feature is that this 3D plasmonic nanogap has a high ratio of gap-depth to gap-width, which can be more than 30 at the sub-10nm gap to form a nanocavity, benefitting local field enhancement and strong localized surface plasmon resonance.

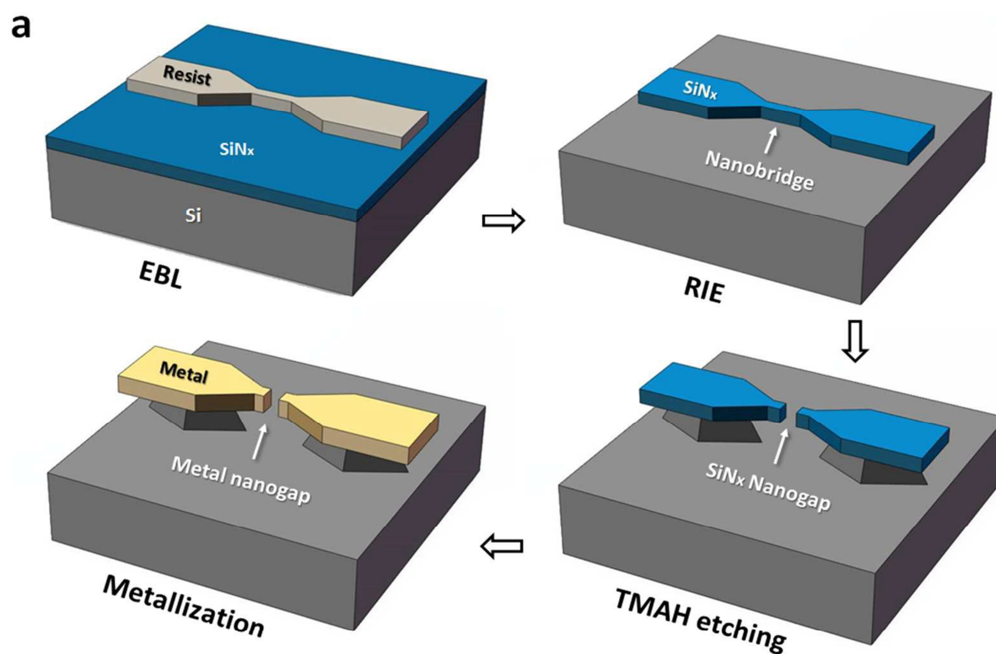

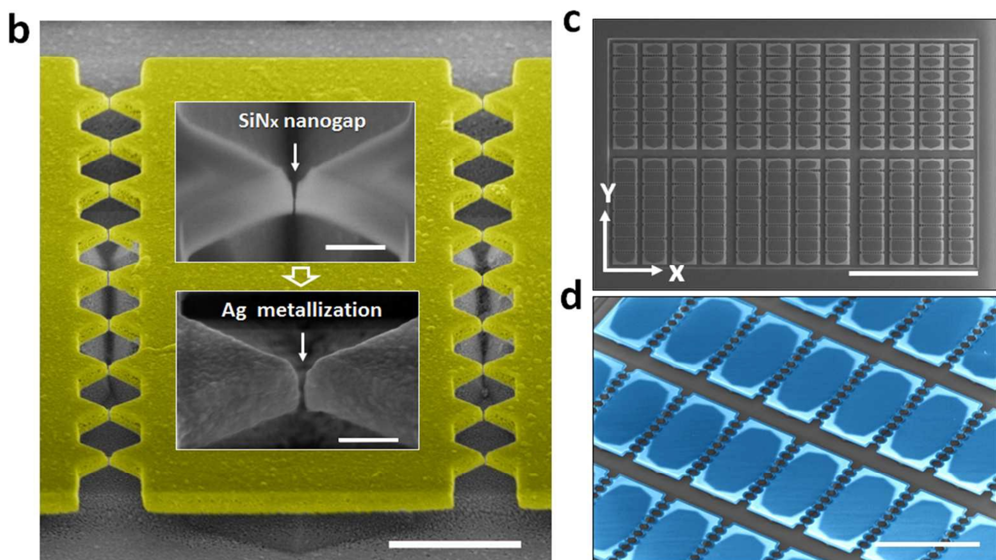

Nanoscale Accepted Manuscript

View Article Online
DOI: 10.1039/C7NR08646F

Figure 1. Stress-induced cracking and metallization doubly controlled method for nanogap fabrication. (a) Schematic of fabrication process from nanobridge to 3D nanogap by EBL, RIE, TMAH etching and Ag metallization. (b) SEM image of two neighboring typically Ag/SiN_x nanogap arrays, in which two insets present enlarged views of a single SiN_x nanogap before and after Ag coating, respectively. The scale bar is 3 μm, and that in the insets is 200 nm. (c) SEM image of a unit of the SiN_x nanogap arrays in an as-fabricated sample with an area of 1×1 cm^2, which includes many nanogap arrays of various sizes, depending upon the nanobridge shape. Scale bar is 100μm. (d) Enlarged SEM image of a section of SiN_x nanogap arrays in (c), and each array includes 9 nanogaps. Scale bar is 10μm.

Figure 1c shows a typical unit of SiN_x nanogap arrays in a large-scale SiN_x nanogap array sample with an area of 1×1 cm^2, which can be easily expanded to larger wafers with distributed multigroup units, each group having an array of nanogaps of a different size. This suggests a mass-fabrication capability. In Figure 1c, the length and width of each nanobridge is designed to be increased and decreased along the marked arrow direction of X and Y to tune the shape of the original nanobridges individually. Nanobridge shape can be used to control nanogap width from above 50nm to sub-10nm in appropriate locations, at which the TMAH etching process determines the cracking effect and hence the width of nanogap. In addition, this 3D nanogap can be customized on demand and reused by wet-etching the metal layer away. An enlarged SEM image of a section of nanogap arrays is exhibited in Figure 1d, in which each array includes 9 nanogaps, and the brightness changes in color of perspective view is due to etching process causing the suspending SiN_x layer. We can see that above fabrication process show good design

Published on 02 January 2018. Downloaded by University of Reading on 07/01/2018 10:39:22.

Nanoscale Accepted Manuscript

View Article Online
DOI: 10.1039/C7NR08646F

controllability in a large area with exact location and number of nanogap, enabling scalable and customized fabrication.

From the above schematic of the fabrication process, we can see that the suspended SiN_x nanogap is the framework of the metallic nanogap, so control in fabricating the SiN_x structure determines the subsequent form of the metallic nanogap. From nanobridge to nanogap, the TMAH etching process that produces the suspended is key, leading to the release of tensile stress that is inherent in the SiN_x nanobridge. Moreover, this causes the concentrated stress in the middle of SiN_x nanobridge. Once the local stress at the middle overcomes the strength of the SiN_x film, a crack appears at the middle of the nanobridge. Figure 2a is an SEM image of a SiN_x nanobridge with fixed width and length before the TMAH etching process, so no nanogap appears. For this un-suspended SiN_x nanobridge, a simulation of stress distribution based on maximum principal stress was carried out by the finite elements method (FEM), as shown in Figure 2b. We can see that the stress is concentrated at the center of the nanobridge, which suggests the most likely breaking site is on the nanobridge. As a result of the stress release during the TMAH etching, the nanogap appears in the middle of the nanobridge, as shown in Figure 2c, which is a SEM image of a typical array of suspended SiN_x nanogaps induced by released stress. From Figure 2c, we find that the nanogap width has little variation from the side to the middle in this array, although the etched parts under the nanogap have an evident difference between the side and middle of this nanogap array. To explain this phenomenon, the displacement distribution in a nanogap array after the stress has been released was simulated by FEM, as shown in Figure 2d, suggesting that the nanobridges in an array couple with each other, leading to almost uniform width in an array. Figure 2e indicates better agreement between the simulated (black rectangle) and experimental (empty circle) results for gap width in an array of

Published on 02 January 2018. Downloaded by University of Reading on 07/01/2018 10:39:22.

Nanoscale Accepted Manuscript

View Article Online
DOI: 10.1039/C7NR08646F

Figure 2c. Although the gap width at the sides is only approximately 6% larger than the center one, the nanogaps in an array still show a considerable uniformity.

Dependencies of the SiN_x nanogap on the length and width of nanobridge are summarized in Figure 2f. We can see that the nanogap increases with increasing bridge-length at a fixed bridge-width, but an inverse trend is seen that the nanogap decreases with increasing bridge-width at a fixed bridge-length. As bridge-length varies, the sample with a 20 nm wide bridge changes more than other samples do, indicating that narrower bridge width is more critical to nanogap formation when the bridge-length varies. Therefore, this cracking-induced nanogap depends on the variation of the shape of nanobridges controlled by not only their length, but also width, which is very different from a previous report.[40] In this work, we propose that the shape of the nanobridge is composed of its length (X) and width (Y) defined in the Figure.2a, determining the width of SiN_x nanogap (W). When the Si substrate below the nanobridge is etched along both vertical and lateral directions, the concentration and release of stress lead to the formation of a nanogap, and its width (W) can be expressed as: $W=\sigma\cdot S(X,Y)\cdot(1-\upsilon)/E$. Where σ, E and υ are the stress, Young's Modulus, and Poisson's ratio of the SiN_x film, respectively, and $S(X, Y)$ is a shape function that is related with the length (X) and width (Y) of the nanobridge and determines the size of the etched area below nanobridge. Practically, with increasing bridge length (X) and decreasing bridge width (Y), more Si below the nanobridge could be etched away, and $S(X, Y)$ tends to be larger, and gap width (W) enlarged as a result. Thus, the gap width can be well defined by $S(X, Y)$ controlling the etched amount of Si below the nanobridge, and moreover, this also explains the change mechanism of the nanogap with the length and width of the nanobridge shown in Figure 2d.

Published on 02 January 2018. Downloaded by University of Reading on 07/01/2018 10:39:22.

Nanoscale Accepted Manuscript

View Article Online
DOI: 10.1039/C7NR08646F

Published on 02 January 2018. Downloaded by University of Reading on 07/01/2018 10:39:22.

Nanoscale Accepted Manuscript

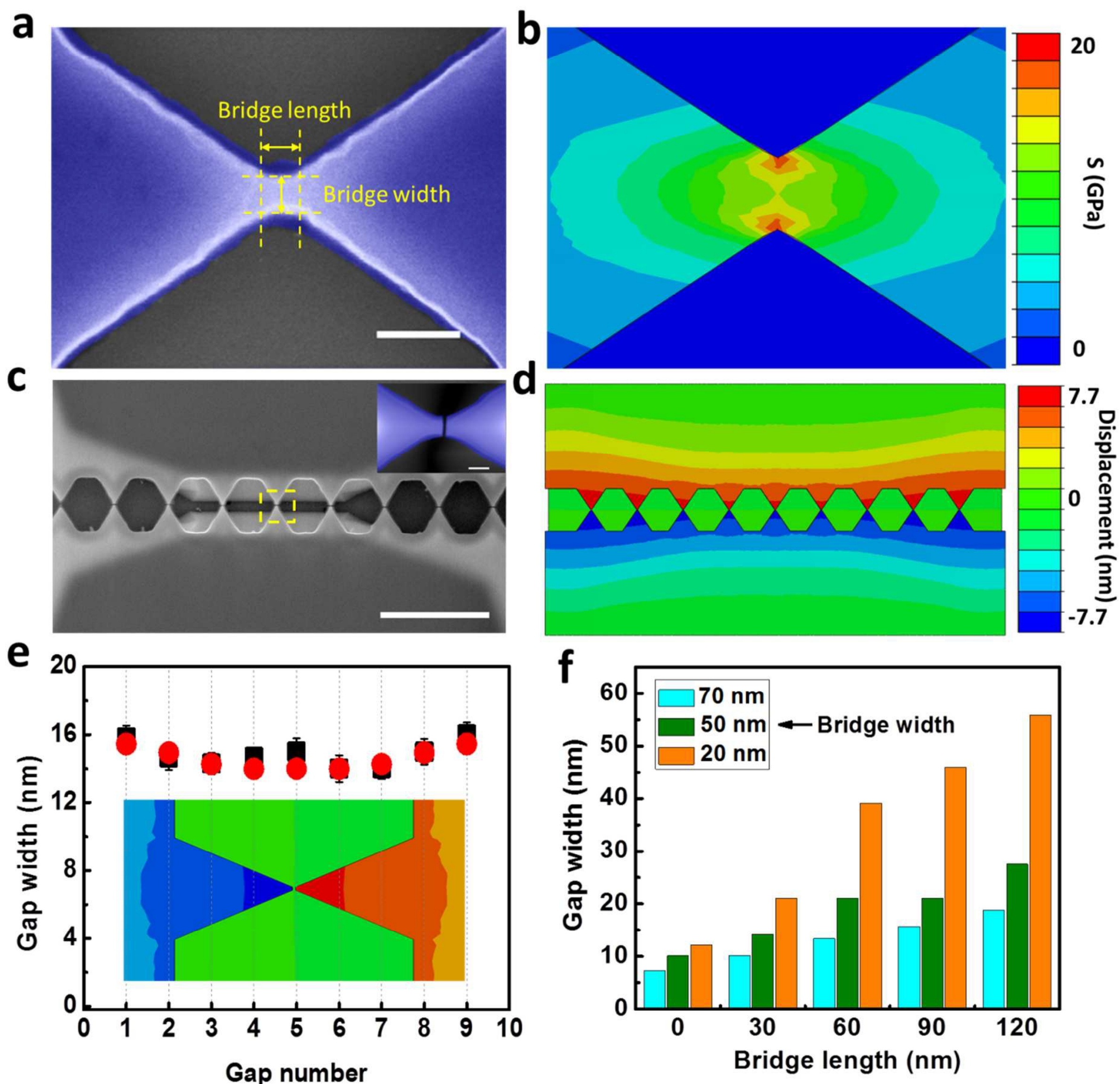

Figure 2. (a) SEM image of a single SiN_x nanobridge before TMAH etching process, in which the shape of a nanobridge is determined by itself width and length defined by dash-line. Scale bar 100 nm. (b) Maximum principal stress distribution of this single nanobridge. (c) SEM image of a typical suspend SiN_x nanogap array with 9 nanogaps after etching process, in which the stress has been released. An inset shows an enlarged single nanogap in the middle of this array, as marked by dash-line. Scale bar 2 μm and 100 nm. (d) The simulated displacement distribution

View Article Online
DOI: 10.1039/C7NR08646F

in this nanogap array corresponding to (c). (e) Comparison results from simulated (black rectangle) and experimental (empty circle) of the width of each gap in this array. An inset shows a magnified view of a single SiN_x gap selected from (d). (f) Nanogap width (*W*) as a function of the width (*X*) and length (*Y*) of the nanobridge.

Published on 02 January 2018. Downloaded by University of Reading on 07/01/2018 10:39:22.

Metallization is a key step to functionalize SiN_x nanogaps and form metal nanogaps. Here, a high-quality smooth Ag film with roughness of 2.3 nm (RMS) is coated on the SiN_x nanogap arrays for metallization. The Ag deposition can narrow the SiN_x nanogap to sub-10 nm by partly filling it with Ag film, finally forming the desired Ag/SiN_x nanogap. Figure 3a compares the width of SiNx nanogap in a single array with 9 gaps before and after Ag deposition, and this array is chosen freely from large-area nanogap arrays shown in Figure 1c and 1d. We can see that 9 SiN_x nanogaps with the same width of ~30nm in one array (blue column) can be shrunk to a sub-10 nm gap (Red column) by depositing ~25nm thick Ag layer, reflecting the uniformity and reliability of this metallization process. Moreover, SiN_x gaps, with different widths in the range of 20 ~ 50nm, can be tuned to form sub-10 nm metallic nanogaps by adjusting the thickness of Ag coating between 20 and 60nm, as shown in Figure 3b, which indicates a linear dependence of metal gap width on the SiN_x gap at different Ag thicknesses. Figure 3c exhibits the morphologies of three typical sub-10 nm Ag/SiN_x nanogaps selected from Figure 3b, such as 7.8 nm, 8.5 nm and 9.6 nm. We can see that SiN_x gaps of various sizes can be shrunk down to sub-10 nm by controlling Ag deposition, implying stability and controllability of this metallization process. From Figure 1 to Figure 3, we confirmed the feasibility of stress-cracking and metallization together controlling 3D suspended nanogaps, further demonstrating a reproducible, scalable and large-scale fabrication of 3D metal nanogap arrays with the gaps' width controllable from sub-10nm to tens of nanometers, providing a reliable, customized way to

Nanoscale Accepted Manuscript

View Article Online
DOI: 10.1039/C7NR08646F

Published on 02 January 2018. Downloaded by University of Reading on 07/01/2018 10:39:22.

mass-produce plasmonic nanogap arrays. Hence the method as a whole is rather conducive to gap-based electronic device applications.

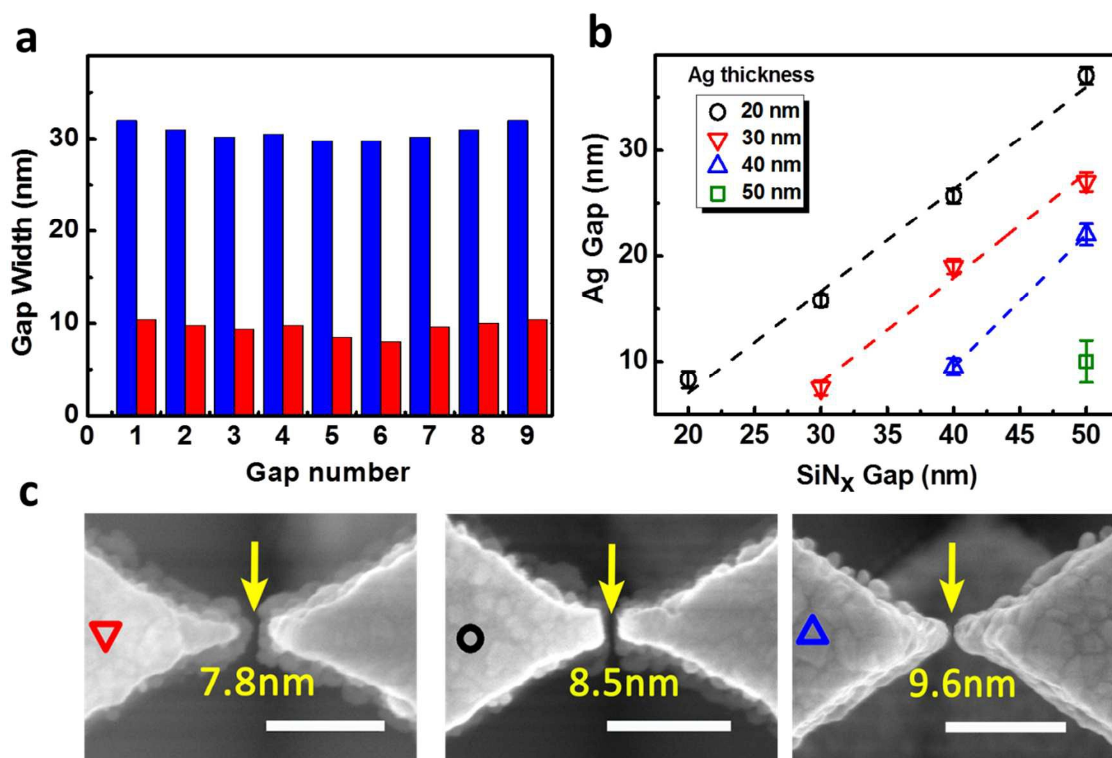

Figure 3. (a) Statistical results of a typical SiN_x nanogap array before and after Ag layer deposition. One SiN_x nanogap array has 9 gaps in number and about 30 nm in width, and sub-10nm Ag nanogap (red column) can be fabricated by depositing a 25 nm Ag layer on SiN_x nanogap (blue column). (b) Dependence of Ag nanogap width on the width of the SiN_x nanogap and the thickness of the Ag layer. (c) SEM images of sub-10 nm Ag gaps obtained on SiN_x nanogaps 20 nm, 30 nm and 40 nm in width by correspondingly depositing Ag film 20 nm, 30 nm ,45 nm, respectively. Scale bar: 100nm.

Suspended plasmonic nanogap array as ultrasensitive SERS substrate

The plasmonic nanogap array structure is a perfect candidate for highly sensitive SERS detection, due to strong electromagnetic field enhancement induced by the nanogap. Here, an as-fabricated

Nanoscale Accepted Manuscript

View Article Online
DOI: 10.1039/C7NR08646F

sample array of suspended 3D Ag/SiN_x nanogaps with ~8nm in width is employed as a SERS probe and the Rhodamine 6 G (R6G) is used as the Raman probe. Each nanogap in a single array can be used as a Raman measurement point for SERS detection with ~2μm size in area. To obtain the sensitivity of these suspended plasmonic nanogaps as a SERS probe, Raman spectra of R6G molecules with concentrations from 10^{-8} M to 10^{-16} M on the suspended nanogaps were successively measured, as shown in Figure 4a. Note that the signal of R6G is still detectable at an extremely low concentration of 10^{-16} M from most of nanogaps, directly demonstrating the remarkable ability of sub-10 nm suspended nanogaps for ultra-sensitive molecular detection. Figure 4b show the dependence of the intensities of two typical R6G characteristic peaks at 613 cm^{-1} and 1366 cm^{-1} on the concentration, revealing a linear dependence of intensity on the concentrations. To further examine the sensitivity of 3D nanogaps, SERS spectra of R6G at 10^{-16} M on the same nanogap array were collected after immersing time for 3 h, 6 h, 9 h, and 12 h, respectively. From Figure 4c, we can see that the intensity of typical R6G characteristic peaks increase gradually as the immersion time increase from 3 hours to 12 hours, and the peaks at 613 cm^{-1}, 775 cm^{-1} and 1366 cm^{-1} become distinguishable after 6 hours and strong after 12 hours, which suggests that the number of absorbed molecules increases with time. Corresponding to Figure 4c, a near-linear dependence of the peaks intensities at 613 cm^{-1} and 1366 cm^{-1} on immersion time is further evidence that the nanogap array-covered surface has ultra-sensitive capability to detect molecules, as shown in Figure 4d. Then, the uniformity of SERS spectra are tested by collecting Raman spectra for R6G in 10^{-16} M solution from five nanogaps on a single random nanogap array, as shown in Figure 4e, in which most typical R6G characteristic peaks can still be distinguished clearly, sufficiently demonstrating the homogeneity of extreme detection ability of suspended nanogaps. In order to examining the spatial distribution of the

Published on 02 January 2018. Downloaded by University of Reading on 07/01/2018 10:39:22.

Nanoscale Accepted Manuscript

View Article Online
DOI: 10.1039/C7NR08646F

Published on 02 January 2018. Downloaded by University of Reading on 07/01/2018 10:39:22.

localized field enhancement and the homogeneity of SERS response, Raman mapping was performed on a nanogap array prepared in the R6G solution at 10^{-8} M. The Raman mapping image was created using the sum of peak intensities at 613 cm^{-1}, 775 cm^{-1} and 1366 cm^{-1}. As can be seen in Figure 4f, the mapping image is a clear profile of the nanogap array, which overlays well with the optical image. Notably, the highest SERS intensity was found at the nanogap, implying that hot spots locate only at the nanogap zone. The mapping results certainly demonstrate that the strong electric field enhancement is localized entirely at the gap zone, as well as showing the controllability and repeatability of the fabrication process. In addition, one can see that the areas aside of the suspended nanogap structure also exhibit strong SERS intensity, which would be attributed to the rough surface caused by etching process as a result of the metallization process.

Here, SERS enhancement factor (EF) can be estimated by the conventional formula of $EF = (I_{SERS}/N_{SERS})/(I_{Bulk}/N_{Bulk})$, where I_{SERS} and N_{SERS} are the SERS signal intensity and number of molecules absorbed on the surface of the sample exposed by the laser, while I_{Bulk} and N_{Bulk} are the Raman signal intensity and number of molecules of R6G powder exposed by laser. The generally accepted notion is that when a sample is immersed in 10^{-4} M concentration R6G for 3 hours, a monolayer of R6G absorbs on the sample surface. [41, 42] Then N_{SERS} can be calculated by $N_{SERS}=S/S_{R6G}$, S and S_{R6G} are the area of sample exposed by laser and the occupied area of a R6G molecule, respectively. Besides, $N_{bulk} = M/m = (S_{spot} \cdot L \cdot \rho \cdot N_A)/m_{mol}$, where M and m are the mass of excited R6G powder and molecular mass of R6G, respectively. L is the depth of laser penetration in R6G, ρ is the density of R6G, and S_{spot} is an area of laser sopt with 1μm radius, N_A is Avogadro number, and m_{mol} is the molar mass of R6G. The calculation results indicate that the SERS EF of R6G in the suspended 8 nm Ag/SiN_x nanogap structure can be estimated to be $\sim 10^8$,

Nanoscale Accepted Manuscript

View Article Online
DOI: 10.1039/C7NR08646F

higher than the SERS EF reported by using other nanofabrication processes. Such a high SERS EF value for 3D nanogap is the reason that we obtain an extremely high-sensitivity of 10^{-16} M in SERS detection, while holding promise for SERS detection even at a single-molecule level.[43]

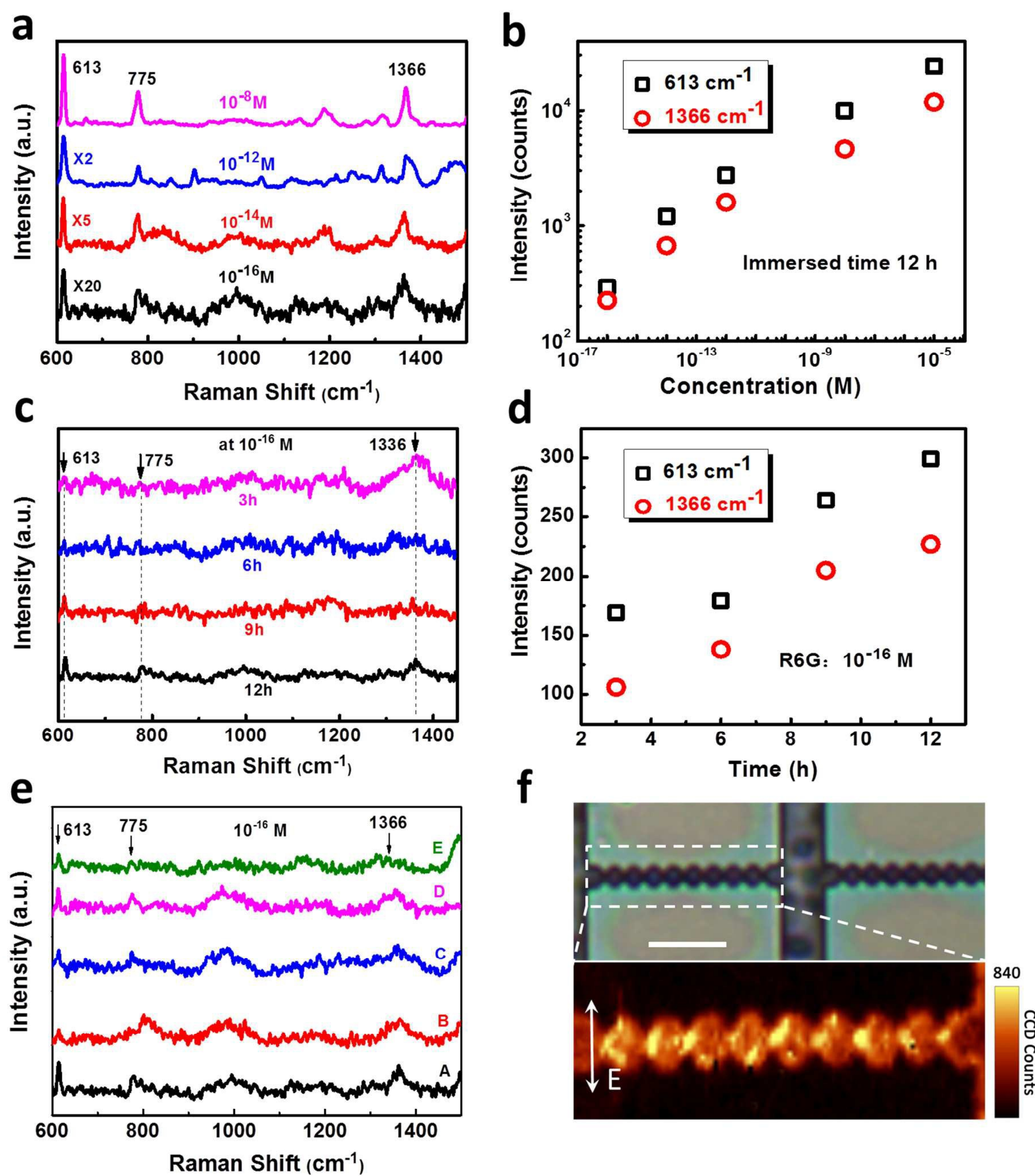

Published on 02 January 2018. Downloaded by University of Reading on 07/01/2018 10:39:22.

Nanoscale Accepted Manuscript

View Article Online
DOI: 10.1039/C7NR08646F
Published on 02 January 2018. Downloaded by University of Reading on 07/01/2018 10:39:22.
Nanoscale Accepted Manuscript

Figure 4. (a) SERS spectra of R6G with different concentrations ranging from 10^{-8} M to 10^{-16} M, all from one single nanogap under the same immersion time. To make this graph visually clear, the spectra of 10^{-14} M and 10^{-16} M are multiplied by 5 and 20. (b) The intensity of the Raman feature peak of the R6G at 613 cm^{-1} and 1366 cm^{-1} as a function of molecular concentration from 10^{-8} to 10^{-16} M (in log scale), corresponding to (a). (c) SERS spectra of the same gap with a 10^{-16} M R6G were collected after immersion for 3 h, 6 h, 9 h, and 12 h. (d) the change of the intensity of the Raman feature peak of the R6G at 613 cm^{-1} and 1366 cm^{-1} with immersion time, corresponding to (c). (e) SERS spectra collected from five sub-10 nm nanogaps in a single random array prepared at a R6G solution of 10^{-16} M, showing a good uniformity. (f) Raman optical image(top) of typical nanogap arrays and corresponding Raman mapping image (bottom) of a nanogap array created using the sum of peak intensities at 613 cm^{-1}, 775 cm^{-1} and 1366 cm^{-1}, at a R6G solution of 10^{-8} M. Scale bar: 2 μm.

Field enhancement mechanism

For as-fabricated 3D plasmonic nanogap, sub-10nm gap is very important feature that can of produce a very strong field enhancement effect that contributes mainly to ultrasensitive detection. Moreover, a large ratio of gap-height to gap-width (more than 30) is another outstanding feature, which forms a deep nanocavity below the Ag-nanogap to confine photons and further increase the field enhancement in the gap zone. Thus, such a deep plasmonic nanogap will have an advantage in local field enhancement over a shallow nanogap. Figure 5 shows the FDTD simulation results of electromagnetic field distribution of sub-10nm suspended 3D Ag/SiN_x gap, clarifying the mechanism of field enhancement and the concentrated effect on the light in a deep nanocavity below the nanogap. As shown in Figure 5a, the 8 nm metallic nanogap formed by coating a 25 nm Ag layer over a SiN_x nanogap with 220 nm in depth was chosen as a basic

View Article Online
DOI: 10.1039/C7NR08646F

Published on 02 January 2018. Downloaded by University of Reading on 07/01/2018 10:39:22.

model structure. Figure 5b illustrates the field distribution on a suspended Ag/SiN_x nanogap above a V-shaped cavity, and here one can see clearly that the maximum value of the enhanced field is localized entirely between the two Ag tips. Figures 5c and 5d give X-Z and X-Y enlarged views, respectively, of the electric field amplitude distribution in a single Ag-nanogap, in which the strongest field enhancement clearly appears in the top of the Ag nanogap and in the center between the Ag tips, contributing greatly to ultrasensitive SERS detection. Besides, Ag nanoparticles around the nanogap also have contribution to the SERS effect. The depth of the SiN_x gap, with a high aspect ratio forming a vertical nanocavity, must be another key factor influencing the field enhancement of the suspended Ag nanogap. It has been demonstrated that the nanocavity structure helps magnify the electric field coupling in the nanogap,[23, 44] by squeezing the phonon in a small volume. Thus, this nanocavity enhances the plasmon coupling in the gap zone, leading to higher SERS intensity in the nanogap.

In this work, the depth of a nanocavity is determined by the thickness of the SiN_x layer. Figure 5e presents FDTD simulation results of field distribution at different thicknesses from 100 nm to 300 nm of SiN_x layer, one-to-one corresponding to the depth of SiN_x gap, so we can clearly distinguish the effect of the SiN_x gap's depth on the field enhancement of the Ag nanogap by brightness differences of the spots dispersed in the nanocavity. By examining the field distribution along the Ag/SiN_x gap, we can see that a gap depth of 220nm shows the strongest field intensity, focused mainly around the upper end of the gap. Moreover, the field intensity distribution along the gap varies somewhat in brightness with change in the gap depth. Overall, this trench is covered with Ag and forms a line of gap by two slanted side walls, which can generate strong local electric field and couple with the LSPR from the nanogap of top Ag. Further, we infer that such a nanocavity can be considered as a nano-waveguide structure

Nanoscale Accepted Manuscript

View Article Online
DOI: 10.1039/C7NR08646F

composed of the upper Ag nanogap and the lower SiN_x deep nanogap. When an incident light beam enters into this nano-waveguide structure through the metal nanogap, the light produces a series of reflectance and interference effects, causing a Fabry-Perot resonance. In this kind of resonance, the field intensity distribution differs according to the gap depth at the nanocavity, which accords well with the simulated field intensity distribution shown in Figure 5e.

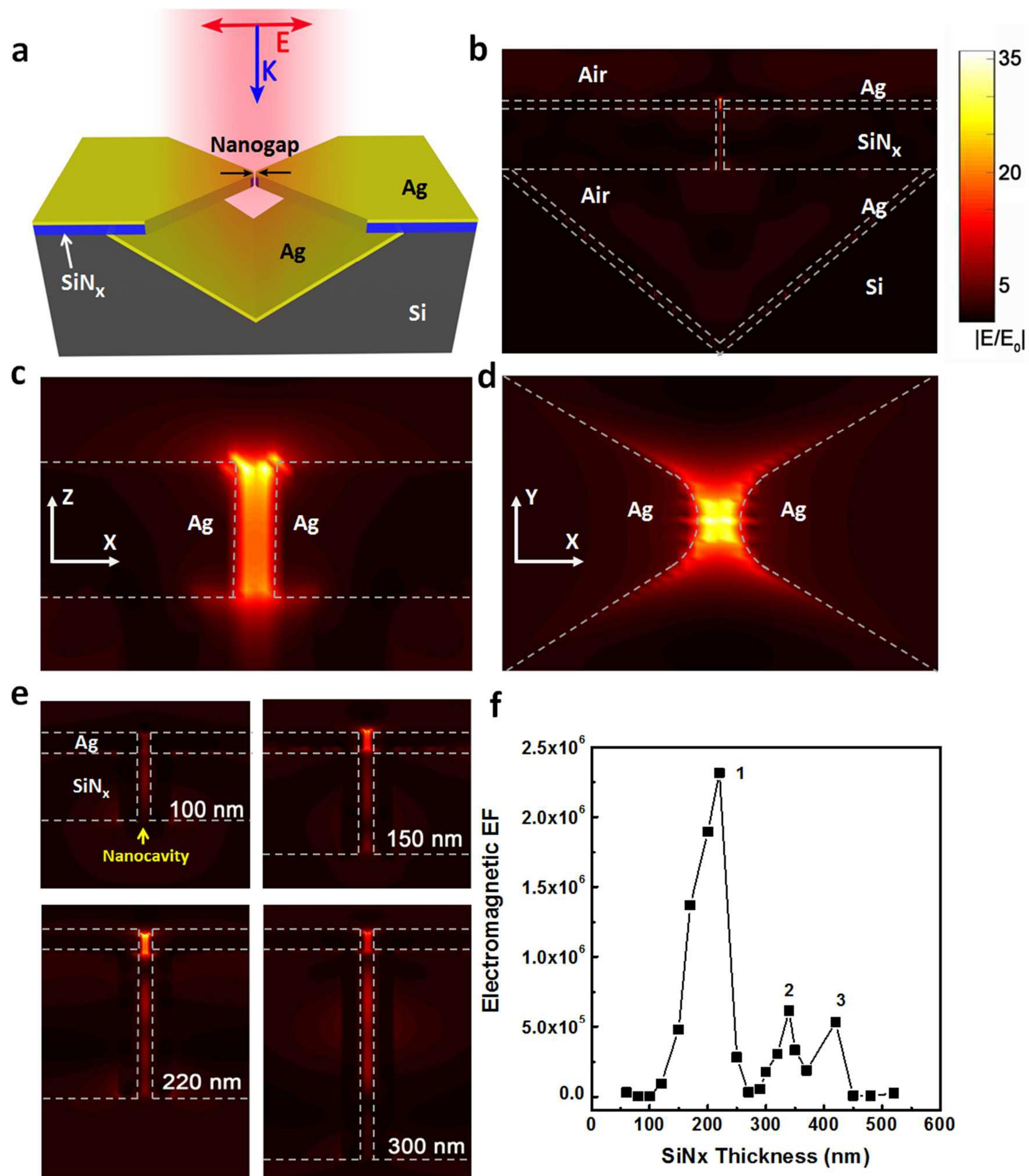

Published on 02 January 2018. Downloaded by University of Reading on 07/01/2018 10:39:22.

Nanoscale Accepted Manuscript

View Article Online
DOI: 10.1039/C7NR08646F

Figure 5. (a) Schematic of the structure of the 3D suspended Ag/SiN_x nanogap. (b) Cross-sectional view of the calculated electric field distribution in a suspended Ag/SiN_x nanogap. (c) and (d) Magnified X-Z and X-Y views of the electric field distribution in the Ag nanogap. (e) Electric field distribution profiles of the suspended Ag/SiN_x nanogap with 100 nm, 150 nm 220 nm and 300nm thick SiN_x layer, respectively; (f) Dependence of the field enhancement factor (EF) of Ag nanogap on SiN_x layers of different thicknesses, indicating a Fabry-Perot resonance occurring in such a nanocavity structure.

In order to further verify the existence of Fabry-Perot resonance in such a nanocavity, the simulated electromagnetic enhancement factor (EF) of the Ag nanogap is plotted for different SiN_x gap depths in Figure 5f. The curve in the Figure 5f shows a clear fluctuation, and the highest EF of 2.3×10^6 appears at a gap depth of 220 nm and then decreases with decreasing gap depth. Interestingly, two other peak values of EF can be observed at gap depths of 340 nm and 420 nm, showing a quasi-periodic change feature. The variation of EF with gap depth, given in the Figure 5f, complies with the characteristics of Fabry-Perot resonance sufficiently to prove that this resonance occurs in such a nanogap structure. For Fabry-Perot resonance, if the depth of the nanocavity and the wavelength of the light are well matched, the EF value reaches a maximum due to a resonance dominated by constructive interference, otherwise, the EF value tends toward a minimum when a resonance is dominated by destructive interference.[24, 33, 45] Therefore, for such 3D suspended Ag/SiN_x nanogaps considered as plasmonic nanocavities with high aspect ratio, an appropriate gap depth (220 nm) is highly conducive to greatly enhanced local field intensity in the nanocavity and especially in the Ag nanogap, due to Fabry-Perot resonance occurring in the nanocavity, which contributes greatly to ultrasensitive SERS detection in this work. Notably, above simulated electromagnetic EF is smaller than pervious

Published on 02 January 2018. Downloaded by University of Reading on 07/01/2018 10:39:22.
Nanoscale Accepted Manuscript

View Article Online
DOI: 10.1039/C7NR08646F

calculated SERS EF, which can be attributed to the fact that the electromagnetic EF simulation can't reflect two contributions from both chemical enhancement and the rough surface of Ag film to enhance the SERS signal, compared with SERS EF.

Conclusions

In this work, we present a feasible approach to fabricate sub-10 nm suspended plasmonic metallic nanogaps with extreme geometries by combining stress-induced cracking with metallization. The fabrication method has a good controllability for the location, number and size of nanogap formation in a large area, and can produce large numbers of nanogap array devices on a surface with good uniformity. Such a 3D plasmonic nanogap is used as the SERS substrate, showing extremely high sensitivity of ~10^{-16} M to R6G molecules and a very strong SERS enhancement factor of ~10^8, demonstrating extraordinary SERS detection ability even at single molecules level and great potential for application in ultra-sensitive detection devices. Based on FDTD simulation, interestingly, we find that a Fabry-Perot resonance occurs at a deep nanocavity beneath the nanogap structure, greatly enhancing local field intensity, especially in the Ag nanogap sample with the highest electromagnetic EF of 2.3×10^6, at a gap depth of 220 nm, which is the main contributor to the ultrasensitive SERS detection demonstrated in this work. Also, this 3D metallic nanogap is a good candidate for nanoelectrodes serving as building blocks for electronic measurement devices. The nanocracking followed by metallization prove to be a stable, repeatable, and efficient way to fabricate suspended sub-10 nm gaps over large area and opens up a route for such an array's practical application in molecular devices and sensing, and even more promising areas.

Conflicts of interest

Published on 02 January 2018. Downloaded by University of Reading on 07/01/2018 10:39:22.

Nanoscale Accepted Manuscript

View Article Online
DOI: 10.1039/C7NR08646F

Published on 02 January 2018. Downloaded by University of Reading on 07/01/2018 10:39:22.

Nanoscale Accepted Manuscript

The authors declare no competing financial interest.

Acknowledgments

The authors acknowledge the financial support from the Ministry of Science and Technology of China (Grant No. 2016YFA0200800, 2016YFA0200400 and 2016YFB0100500), the National Natural Science Foundation of China (Grant No. 11674387, 91323304, 11704401, 61390503, 11574385, and 11574368) and the "Strategic Priority Research Program" of the Chinese Academy of Sciences (Grant No. XDB07020200).

References

1. J. Semple, S. Rossbauer, C. H. Burgess, K. Zhao, L. K. Jagadamma, A. Amassian, M. A. McLachlan and T. D. Anthopoulos, *Small*, 2016, **12**, 1993-2000.
2. W. Zhu, M. G. Banaee, D. Wang, Y. Chu and K. B. Crozier, *Small*, 2011, **7**, 1761-1766.
3. S. Si, W. Liang, Y. Sun, J. Huang, W. Ma, Z. Liang, Q. Bao and L. Jiang, *Adv. Funct. Mater.*, 2016, DOI: 10.1002/adfm.201602337.
4. M. Parzefall, P. Bharadwaj, A. Jain, T. Taniguchi, K. Watanabe and L. Novotny, *Nature nanotechnology*, 2015, **10**, 1058-1063.
5. H. Song, M. A. Reed and T. Lee, *Adv. Mater.*, 2011, **23**, 1583-1608.
6. J. O. Lee, Y. H. Song, M. W. Kim, M. H. Kang, J. S. Oh, H. H. Yang and J. B. Yoon, *Nature nanotechnology*, 2013, **8**, 36-40.
7. Q. Zhao, W. Wang, J. Shao, X. Li, H. Tian, L. Liu, X. Mei, Y. Ding and B. Lu, *Adv. Mater.*, 2016, **28**, 6337-6344.
8. W. Cai, J. S. White and M. L. Brongersma, *Nano Lett.*, 2009, **9**, 4403.
9. T. Yelin, R. Korytar, N. Sukenik, R. Vardimon, B. Kumar, C. Nuckolls, F. Evers and O. Tal, *Nature materials*, 2016, **15**, 444-449.
10. M. Di Ventra and M. Taniguchi, *Nature nanotechnology*, 2016, **11**, 117-126.
11. B. Jang, K. Y. Lee, J.-S. Noh and W. Lee, *Sensors Actuators B: Chem.*, 2014, **193**, 530-535.

View Article Online
DOI: 10.1039/C7NR08646F

Published on 02 January 2018. Downloaded by University of Reading on 07/01/2018 10:39:22.

12. L. V. Brown, X. Yang, K. Zhao, B. Y. Zheng, P. Nordlander and N. J. Halas, *Nano Lett.*, 2015, **15**, 1272-1280.
13. D. Kang, P. V. Pikhitsa, Y. W. Choi, C. Lee, S. S. Shin, L. Piao, B. Park, K. Y. Suh, T. I. Kim and M. Choi, *Nature*, 2014, **516**, 222-226.
14. Z. Hu, Z. Liu, L. Li, B. Quan, Y. Li, J. Li and C. Gu, *Small*, 2014, **10**, 3933-3942.
15. J. Leem, M. C. Wang, P. Kang and S. Nam, *Nano Lett.*, 2015, **15**, 7684-7690.
16. A. Toma, S. Tuccio, M. Prato, F. De Donato, A. Perucchi, P. Di Pietro, S. Marras, C. Liberale, R. Proietti Zaccaria, F. De Angelis, L. Manna, S. Lupi, E. Di Fabrizio and L. Razzari, *Nano Lett.*, 2015, **15**, 386-391.
17. C. Zhu, G. Meng, P. Zheng, Q. Huang, Z. Li, X. Hu, X. Wang, Z. Huang, F. Li and N. Wu, *Adv. Mater.*, 2016, **28**, 4871-4876.
18. J. Zhang, M. Irannejad and B. Cui, *Plasmonics*, 2014, **10**, 831-837.
19. N. A. Hatab, C. H. Hsueh, A. L. Gaddis, S. T. Retterer, J. H. Li, G. Eres, Z. Zhang and B. Gu, *Nano Lett.*, 2010, **10**, 4952-4955.
20. D. Natelson, Y. Li and J. B. Herzog, *Phys. Chem. Chem. Phys.*, 2013, **15**, 5262-5275.
21. X. Liu, D. Wu, Q. Chang, J. Zhou, Y. Zhang and Z. Wang, *Nanoscale*, 2017, **9**, 15390-15396.
22. Z. Xie, S. Feng, P. Wang, L. Zhang, X. Ren, L. Cui, T. Zhai, J. Chen, Y. Wang and X. Wang, *Advanced Optical Materials*, 2015, **3**, 1232-1239.
23. M. K. Kim, H. Sim, S. J. Yoon, S. H. Gong, C. W. Ahn, Y. H. Cho and Y. H. Lee, *Nano Lett.*, 2015, **15**, 4102-4107.
24. X. Chen, H. R. Park, M. Pelton, X. Piao, N. C. Lindquist, H. Im, Y. J. Kim, J. S. Ahn, K. J. Ahn, N. Park, D. S. Kim and S. H. Oh, *Nature communications*, 2013, **4**, 2361.
25. S. Chen, S. Jin and R. Gordon, *Physical Review X*, 2014, **4**.
26. N. A. Abu Hatab, J. M. Oran and M. J. Sepaniak, *ACS Nano*, 2008, **2**, 377-385.
27. W. Yue, Y. Yang, Z. Wang, L. Chen and X. Wang, *The Journal of Physical Chemistry C*, 2013, **117**, 21908-21915.
28. A. Otto, *J. Raman Spectrosc.*, 2006, **37**, 937-947.
29. J. Chen, G. Qin, J. Wang, J. Yu, B. Shen, S. Li, Y. Ren, L. Zuo, W. Shen and B. Das, *Biosens. Bioelectron.*, 2013, **44**, 191-197.

Nanoscale Accepted Manuscript

View Article Online
DOI: 10.1039/C7NR08646F

Published on 02 January 2018. Downloaded by University of Reading on 07/01/2018 10:39:22.

Nanoscale Accepted Manuscript

30. H. Lee, G. H. Kim, J. H. Lee, N. H. Kim, J. M. Nam and Y. D. Suh, *Nano Lett.*, 2015, **15**, 4628-4636.
31. X. Chen, N. C. Lindquist, D. J. Klemme, P. Nagpal, D. J. Norris and S. H. Oh, *Nano Lett.*, 2016, **16**, 7849-7856.
32. Q. Xiang, X. Zhu, Y. Chen and H. Duan, *Nanotechnology*, 2016, **27**, 075201.
33. D. Yoo, N. C. Nguyen, L. Martin-Moreno, D. A. Mohr, S. Carretero-Palacios, J. Shaver, J. Peraire, T. W. Ebbesen and S. H. Oh, *Nano Lett.*, 2016, **16**, 2040-2046.
34. J. Zhao, M. Sun, Z. Liu, B. Quan, C. Gu and J. Li, *Sci. Rep.*, 2015, **5**, 16019.
35. S. Marqués-González, R. Matsushita and M. Kiguchi, *Journal of Optics*, 2015, **17**, 114001.
36. H. Ni, M. Wang, T. Shen and J. Zhou, *ACS Nano*, 2015, **9**, 1913-1925.
37. L. Lesser-Rojas, P. Ebbinghaus, G. Vasan, M. L. Chu, A. Erbe and C. F. Chou, *Nano Lett.*, 2014, **14**, 2242-2250.
38. J. Tian, B. Liu, X. Li, Z. Yang, B. Ren, S. Wu, N. Tao, and Z. Tian , *J. Am. Chem. Soc.*, 2006, **128**, 14748.
39. S. Pud, D. Verschueren, N. Vukovic, C. Plesa, M. P. Jonsson and C. Dekker, *Self-Aligned Plasmonic Nanopores by Optically Controlled Dielectric Breakdown*, 2015.
40. V. Dubois, F. Niklaus and G. Stemme, *Adv. Mater.*, 2016, **28**, 2178-2182.
41. J. Chen, B. Shen, G. Qin, X. Hu, L. Qian, Z. Wang, S. Li, Y. Ren and L. Zuo, *The Journal of Physical Chemistry C*, 2012, **116**, 3320-3328.
42. W. Yue, Z. Wang, J. Whittaker, F. Lopez-royo, Y. Yang and A. V. Zayats, *Journal of Materials Chemistry C*, 2017, **5**, 4075-4084.
43. E. C. Le Ru and P. G. Etchegoin, *Annu. Rev. Phys. Chem.*, 2012, **63**, 65-87.
44. M. Chirumamilla, A. Toma, A. Gopalakrishnan, G. Das, R. P. Zaccaria, R. Krahne, E. Rondanina, M. Leoncini, C. Liberale, F. De Angelis and E. Di Fabrizio, *Adv. Mater.*, 2014, **26**, 2353-2358.
45. H. T. Miyazaki and Y. Kurokawa, *Phys. Rev. Lett.*, 2006, **96**, 097401.

View Article Online
DOI: 10.1039/C7NR08646F

Published on 02 January 2018. Downloaded by University of Reading on 07/01/2018 10:39:22.

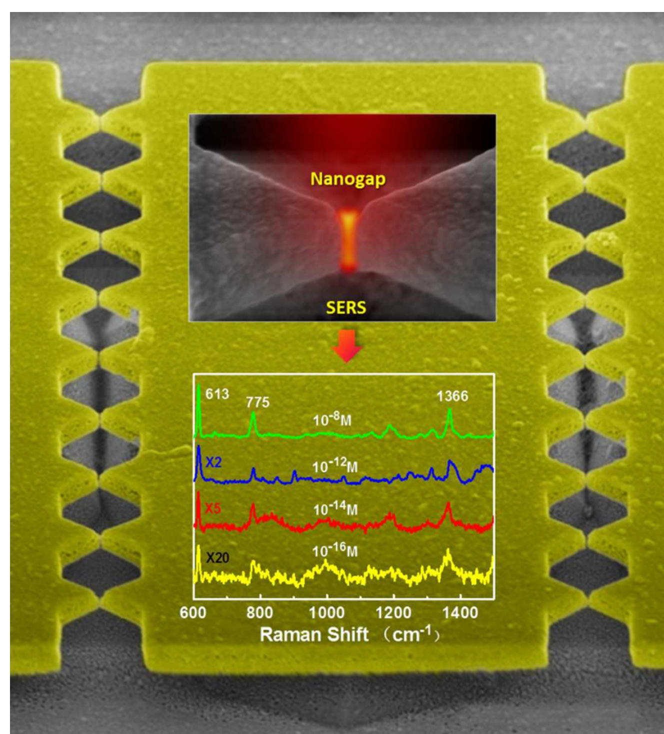

Stress-induced cracking and metallization are combined to fabricate controllably large-scale 3D plasmonic sub-10nm-gap arrays for extremely sensitive SERS detecting application.

Nanoscale Accepted Manuscript